

Electrocatalysis

International Edition: DOI: 10.1002/anie.201907935
German Edition: DOI: 10.1002/ange.201907935In-Situ Nanostructuring and Stabilization of Polycrystalline Copper by an Organic Salt Additive Promotes Electrocatalytic CO₂ Reduction to Ethylene

Arnaud Thevenon, Alonso Rosas-Hernández, Jonas C. Peters,* and Theodor Agapie*

Abstract: Bridging homogeneous molecular systems with heterogeneous catalysts is a promising approach for the development of new electrodes, combining the advantages of both approaches. In the context of CO₂ electroreduction, molecular enhancement of planar copper electrodes has enabled promising advancement towards high Faradaic efficiencies for multicarbon products. Besides, nanostructured copper electrodes have also demonstrated enhanced performance at comparatively low overpotentials. Herein, we report a novel and convenient method for nanostructuring copper electrodes using *N,N'*-ethylene-phenanthroline dibromide as molecular additive. Selectivities up to 70% for C₂₊₂ products are observed for more than 40 h without significant change in the surface morphology. Mechanistic studies reveal several roles for the organic additive, including: the formation of cube-like nanostructures by corrosion of the copper surface, the stabilization of these nanostructures during electrocatalysis by formation of a protective organic layer, and the promotion of C₂₊₂ products.

Introduction

Borrowing concepts from molecular catalysts to tailor the active sites of metallic surfaces and enhance activity, selectivity, and stability has been a long-standing interest in the catalysis community.^[1–4] In the context of the electrochemical CO₂ reduction reaction (CO₂RR), small molecule additives have been employed to tune the reactivity of heterogeneous catalysts by stabilizing intermediates, inhibiting proton diffusion, or acting as redox mediators. For example, organic species such as *N*-aryl pyridinium salts,^[5] imidazole,^[6–8] thiol^[9] and cysteamine^[10] have been reported to alter the surface of the electrode, yielding catalytic systems with increased selectivities for specific products.^[11,12]

Germane to the present study, our research team disclosed a simple method for increasing the selectivity of CO₂RR towards C₂₊₂ products by combining a polycrystalline copper electrode with an *N*-aryl pyridinium salt additive in

bicarbonate aqueous solutions (Figure 1a).^[5] Upon in situ electroreduction of these water-soluble additives, an organic film is deposited onto the electrode, altering the catalytic properties of the Cu surface. Selective inhibition of CH₄ and H₂ production was observed, resulting in an improved selectivity for C₂₊₂ products with Faradaic efficiencies (FE) higher than 60%.

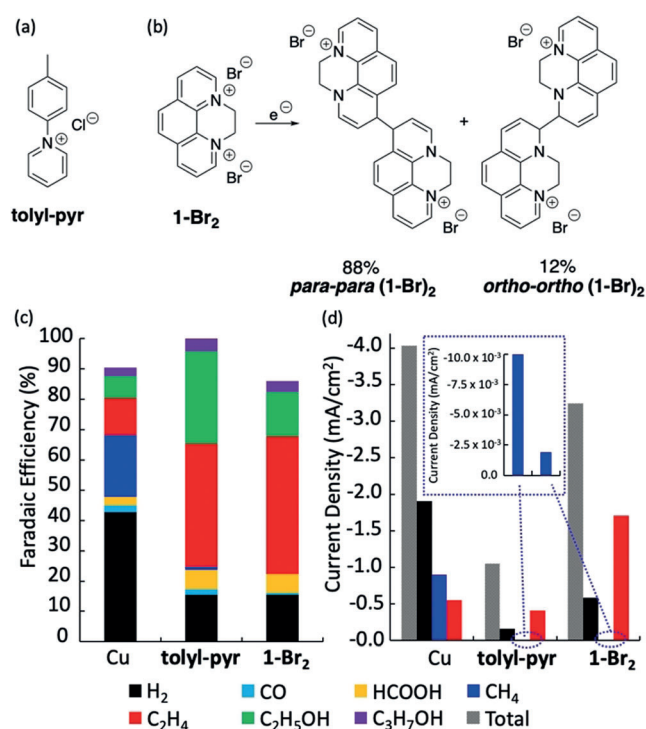


Figure 1. Chemical structure of a) tolyl-pyr, b) 1-Br₂ and its reduction to *para-para* (1-Br)₂ and *ortho-ortho* (1-Br)₂ coupled dimers, respectively. c) Faradaic efficiencies toward different products formed during CO₂RR at -1.07 V in a CO₂-saturated 0.1 M KHCO₃ electrolyte either without, or with, 10 mM of either tolyl-pyr, or 1-Br₂. d) Total and partial current densities for H₂, CH₄ and C₂H₄ without or with 10 mM of either tolyl-pyr or 1-Br₂.

[*] Dr. A. Thevenon, Dr. A. Rosas-Hernández, Prof. Dr. J. C. Peters, Prof. Dr. T. Agapie
Joint Center for Artificial Photosynthesis and Division of Chemistry and Chemical Engineering, California Institute of Technology, Pasadena, California, 91125 (USA)
E-mail: jpeters@caltech.edu
agapie@caltech.edu

Supporting information and the ORCID identification number(s) for the author(s) of this article can be found under <https://doi.org/10.1002/anie.201907935>.

In a complementary approach, nanostructured metal electrodes have played an important role in the development of selective electrocatalysts towards particular products at comparatively low overpotentials.^[13–15] A variety of methods are available to form nanostructures at the surface of electrodes, including reduction of copper oxides, wet chemistry synthesis, and electrodeposition. However, most of these

methods require high-temperature or high-energy treatments and the resulting structures generally exhibit a poorly defined surface morphology.

Specifically, alkali halide salts are known to promote a nanostructuring process in planar Cu electrodes. By exposing the copper surface to an aqueous solution of an alkali halide salt under oxidative potentials or acidic media, nanocube-like structures are obtained. The resulting electrocatalysts show higher current densities and selectivities for ethylene ($20\% < \text{FE}_{\text{C}_2\text{H}_4} < 45\%$) and oxygenated products compared to a planar electrode, although hydrogen is still the predominant product ($40\% < \text{FE}_{\text{H}_2} < 60\%$). Unfortunately, these systems suffer from fast structural reconstruction/degradation and performance decay during catalysis, possibly due to the applied electrochemical bias.^[16–18] As a consequence, the sustained influence of Cu morphology on the resulting products still remains elusive. Therefore, preserving the nanostructures under electrocatalytic conditions is of particular interest as more predictable systems can be developed with increased durability.^[19–26]

To understand the interaction of organic films with Cu electrodes and their impact on catalysis, we have been undertaking structure-function studies on a variety of molecular additives. Herein, we report that combining polycrystalline copper electrodes with *N,N'*-ethylene-phenanthroline dibromide (abbreviated herein as **1-Br₂**, Figure 1 b, Figure S1 in the Supporting Information) provides a particularly robust and conveniently prepared catalytic system that shows improved activity, with current densities up to -7 mA cm^{-2} and selectivities for C_{22} products up to 70%, when compared with an analogous bare polycrystalline copper electrode, or one as previously disclosed using an electrodeposited film derived from *N*-tolylpyridinium chloride (**tolyl-pyr**, Figure 1 a). Mechanistic studies demonstrate that **1-Br₂** plays multiple functions, including the generation of cube-like copper nanostructures, stabilization of the electrode morphology for up to 40 h of electrocatalysis, and to facilitate C–C coupled product formation.

Results and Discussion

Bulk electrolysis experiments were performed on a polycrystalline copper electrode with CO_2 -saturated 0.1 M KHCO_3 electrolyte at pH 6.8 using a recently reported custom flow cell.^[27] Potentials were measured versus a leakless Ag/AgCl electrode and converted to the RHE scale. In the absence of additive and at a potential of $-1.09 \text{ V}_{\text{RHE}}$, the copper electrode primarily produces hydrogen and methane, with relatively low generation of C_{22} products, consistent with previous reports ($\text{FE}_{\text{H}_2} = 43\%$, $\text{FE}_{\text{CH}_4} = 20\%$, $\text{FE}_{\text{C}_{22}} = 22\%$, Figure 1 c and Table S1).^[5,27–29] However, when CO_2RR is performed using an electrolyte containing 10 mM of **1-Br₂**, the selectivity is markedly shifted towards C_{22} products ($\text{FE}_{\text{C}_{22}} = 64\%$, Figure 1 c, Table S1). The selectivity for ethylene is especially enhanced, while methane production is dramatically suppressed ($\text{FE}_{\text{C}_2\text{H}_4} = 45\%$, $\text{FE}_{\text{CH}_4} = 0.5\%$). The use of isotopically labelled $^{13}\text{CO}_2$ confirmed that the sole source of carbon for the observed products is carbon dioxide, ruling out

the possibility of degradation products from the organic additive acting as the carbon source (Figure S2).

Although the selectivity of **1-Br₂** is similar to that we previously reported with **tolyl-pyr** as an organic additive (Figure 1 c,d, $\text{FE}_{\text{C}_{22}} = 78\%$, $j = -1.0 \text{ mA cm}^{-2}$),^[5] the total current density using **1-Br₂** is almost four times higher and similar to that observed with the bare Cu electrode (Figure 1 d, $j = -3.8 \text{ mA cm}^{-2}$ with **1-Br₂**; $j = -4.4 \text{ mA cm}^{-2}$ with bare Cu). This is a drastic difference compared to the first generation of aryl-pyridinium additives we had explored,^[5] where the partial current density for C_{22} products is essentially the same as that of bare Cu, and the shift in selectivity derives from the suppression of H_2 and CH_4 production. For the case of **1-Br₂**, the partial current density for C_{22} products, and especially C_2H_4 , is enhanced almost by a factor of 4 (Figure 1 d).

Higher current densities are achieved at $-1.15 \text{ V}_{\text{RHE}}$ ($j = -6.4 \text{ mA cm}^{-2}$, Figure S3, Table S2) while maintaining similar selectivities for ethylene and C_{22} products ($\text{FE}_{\text{C}_2\text{H}_4} = 40\%$, $\text{FE}_{\text{C}_{22}} = 63\%$, Figure 2, Table S2). Applying additional bias

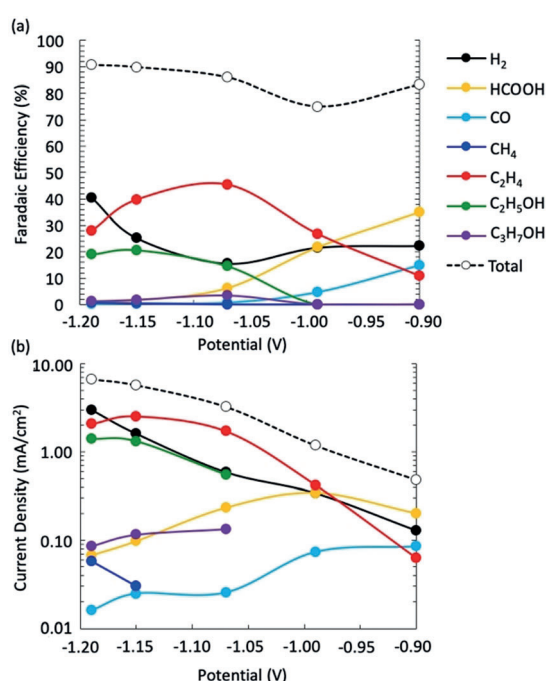


Figure 2. a) Faradaic efficiencies and b) partial current densities for CO_2RR products and hydrogen as a function of potential during CO_2RR in a CO_2 -saturated 0.1 M KHCO_3 electrolyte with 10 mM of **1-Br₂**. Each data point shows the average of three individual measurements.

leads to substantial H_2 generation ($\text{FE}_{\text{H}_2} = 41\%$ at -1.19 V). At lower bias (-0.99 V), ethylene is still a dominant product, together with formic acid ($\text{FE}_{\text{C}_2\text{H}_4} = 27\%$ and $\text{FE}_{\text{HCOOH}} = 22\%$). The CO Faradaic efficiency is still very low at this potential, indicating that the majority of intermediate CO generated is converted to C–C coupled products ($\text{FE}_{\text{CO}} = 4.7\%$). At -0.90 V , ethylene is still produced but with far lower selectivity ($\text{FE}_{\text{C}_2\text{H}_4} = 11\%$). The FE of CO correspondingly increases, and formic acid becomes the major product



generated ($FE_{CO} = 15\%$ and $FE_{HCOOH} = 35\%$). Most notably, at all of these potentials, methane production is almost completely suppressed.

A rather similar product profile is obtained at $-1.07 V_{RHE}$ using concentrations of **1-Br₂** as low as 0.1 mM (Table S3, Figure S4; $FE_{C_2H_4} = 35\%$, $FE_{C_2} = 54\%$), with a similar current density. This observation highlights the strength of the additive effect, even at very low concentrations, on the overall product profile. In addition, the catalytic system shows a sustained high selectivity for ethylene production during longer bulk electrolysis experiments (monitored up to 43 h). A decrease of 10% in ethylene selectivity occurred over this time (Figures S5–S8). This degradation of selectivity potentially comes from deposition of trace metals ion impurities present in the electrolyte, as previously observed.^[30]

Analysis of the electrode surface, after bulk electrolysis using an electrolyte containing **1-Br₂**, by X-ray photoelectron spectroscopy (XPS), showed nitrogen enrichment (Figure S9). The spectrum consists of two peaks of similar area, located at 400.2 eV and 402.5 eV, characteristic of tertiary amine and quaternary ammonium nitrogen atoms, respectively.^[31,32] In addition, the surface of the electrode was rinsed several times with deionized water and then with DMSO-*d*₆. The organic fraction was collected and analyzed by NMR spectroscopy. The ¹H and ¹H-¹H COSY NMR spectra (Figures S10 and S11) acquired are consistent with the formation of two independent dimeric structures, *para-para* (**1-Br**)₂ and *ortho-ortho* (**1-Br**)₂ depicted in Figure 1 b, derived from the coupling of two mono-reduced phenanthroline species (**1-Br**) at the *para* or *ortho* position, respectively. The amount of *para-para* coupled product is higher than the *ortho-ortho* product, as expected from the higher spin density at the *para* position of the precursor radical (Figure S10).^[33] Combined, these species account for >95% of the organic material that could be extracted from the copper electrode.^[34] The results from XPS and NMR analyses are in agreement with the electrodeposition of an organic film onto the surface of the copper electrode, as previously observed in the case of *tolyl-pyr*.^[5]

The dimer (**1-Br**)₂ is a dicationic compound and displays two tertiary and two quaternary amine N-atoms, consistent with the aforementioned XPS results. The copper surface appears to be critical for the dimerization process of the one-electron reduced species of **1-Br₂** (see SI for further discussion). When the one-electron reduced radical **1-Br** is generated in solution using zinc dust as the chemical reductant, the dimerization reaction is not observed. Furthermore, the stability of **1-Br** in the presence of CO₂ was studied by EPR and UV-VIS spectroscopies (Figures S24–S26). The obtained results suggest that radical **1-Br** does not interact with CO₂, ruling out a possible involvement of such a radical during electrocatalysis. Furthermore, when a copper electrode, with dimer (**1-Br**)₂ previously electrodeposited on its surface, is used in bulk electrolysis with an electrolyte free of molecular additive **1-Br₂**, the expected high selectivity for C₂ products is observed (Table S4).

As an organic film is formed on the surface of the electrode, the mass transport limitation of the reactants was studied by chronoamperometry experiments at $-1.10 V$ with

a rotating disk electrode using either a CO₂ or a N₂-saturated 0.1M KHCO₃ electrolyte with or without 10 mM of **1-Br₂** (Figures S12 and S13). Under N₂, the hydrogen current densities are not altered by the rotation speed both on bare Cu or in presence of **1-Br₂**. More interestingly, the hydrogen current density is fivefold lower when the organic film is present, indicating that the film severely inhibits hydrogen production. Under CO₂, the current densities with and without the film are similar at low rotation speed, in agreement with catalytic results. Surprisingly, while the current density increases linearly with the rotation speed on bare Cu, it stays unchanged in the presence of **1-Br₂**. These results demonstrate that there is no apparent mass transport limitation of reactants due to the organic film. These results could reflect different rate determining steps in presence of the film compared to bare Cu, a phenomenon that will be further investigated but is beyond the scope of this study.

To gain information about possible changes in surface morphology of the copper electrode, ex situ scanning electron microscope (SEM) images were taken after different electrocatalytic experiments (Figure 3). A smooth and flat surface is

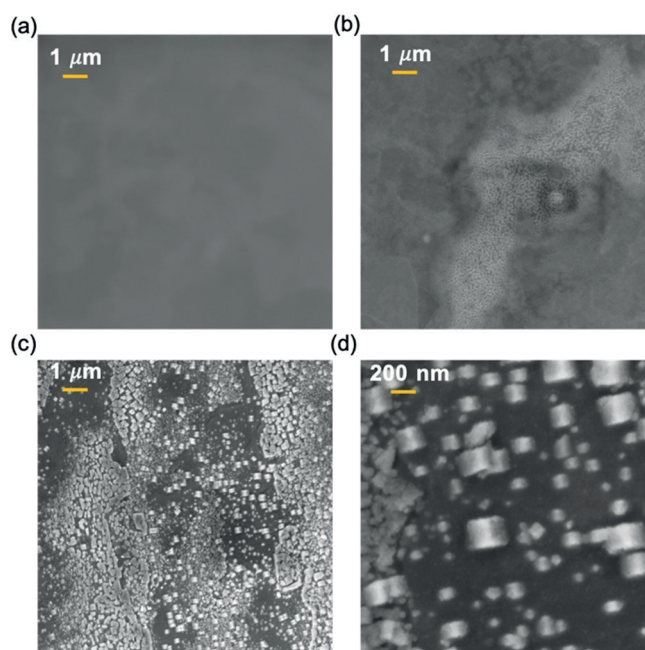


Figure 3. Ex-situ SEM images of four Cu electrodes a) after electropolishing; b) after 65 min of electrocatalysis at $-1.07 V$ in 0.1 M KHCO₃ without **1-Br₂**; c) same as (b), but with 10 mM of **1-Br₂**; d) ex-situ SEM image of the post catalysis electrode from (c), at higher magnification.

consistently observed after electropolishing and prior to electrocatalysis (Figure 3a). When a CO₂RR experiment is performed in the absence of molecular additive, the morphology of the copper electrode after the reaction changes to a rougher surface, as previously reported (Figure 3b).^[35] Notably, when CO₂RR is carried out in the presence of **1-Br₂**, well-defined cubic nanostructures are observed across the entire surface of the copper electrode after catalysis

(Figures 3 c and d). At higher magnification, the ridges of the cubes can be observed and they appear to be parallel to the bulk of the electrode. This suggests that all the nanocubes are growing along the $\langle 110 \rangle$ direction. In addition, as Cu has a face-centered cubic (FCC) packing structure, the exposed surface of such nanostructures has to be dominated by the $\{100\}$ facet. This could not unambiguously be confirmed by analyzing the post-catalysis electrode by bulk XRD as the change in the surface morphology is too small compared to the resolution of the instrument. Nevertheless, by comparing the peak heights of XRD spectra of a freshly electropolished Cu electrode with post catalysis Cu electrodes with and without **1-Br₂**, an increase of the Cu(100) peak is observed in the post-catalysis Cu electrode with **1-Br₂** (Figure S15).

In term of size, the cubic nanostructures display average widths of 275 nm for the biggest ones and 100 nm for the smallest. According to atomic force microscopic (AFM) images, the nanocubes present an average high of 80–90 nm (Figure S14c). SEM energy dispersive X-ray (EDX) analysis confirms that the nanostructures are mainly comprised of copper (Figure S14d).

These structural observations contrast with previous reports on nanostructured copper electrodes.^[16–18] This is the first example of stable copper nanocubes under electrocatalytic conditions over prolonged reaction times (> 40 h, Figure S16). Also, the observed nanocubes after electrocatalysis are well defined and oriented in the same direction, contrasting with the typical morphologies of copper electrodes after catalysis displaying agglomerated nanostructures.

Inorganic halide salts are well known for inducing nanostructuring process in copper surfaces.^[36] Thus, we decided to study the influence of the bromide counteranion in **1-Br₂** on the formation of the observed nanocubes at the electrode surface. When a polycrystalline copper electrode is left in contact with an aqueous solution of KBr (20 mM) for 5 min, and then subjected to 3 measurements of potentiostatic electrochemical impedance spectroscopy (PEIS), AFM images show the presence of nanocubes similar in shape to those formed with additive **1-Br₂**, with a height of ca. 80–90 nm (Figure S17a). This observation suggests that the bromide anion can promote the formation of nanostructures, by a corrosive process,^[37] under our catalytic conditions. It is worth noting that the PEIS measurements were performed at open circuit voltage, resulting in a nanostructuring process under mild conditions. This approach contrasts with the previous reports where high oxidative potentials have been used during the nanostructuring of Cu electrodes.^[37,38]

When KBr (20 mM) was tested as an additive for CO₂RR at -1.07 V_{RHE}, the product profile (Table S5) was similar to that of bare Cu, with hydrogen and methane being the dominant products ($FE_{H_2} = 56\%$, $FE_{CH_4} = 20\%$). Ex-situ post-catalysis AFM images of the electrode indicate a lower level of nanostructuring compared to the case of **1-Br₂** as additive (Figure S17b). These observations allow us to infer that although the organic film is not required for the nanostructuring step, it is critical to preserve the nanocubes during electrocatalysis.

To further explore the role of bromide anion in the nanostructuring process, the surface of a copper electrode was

analyzed by AFM before and after electrocatalysis in the presence of 10 mM of **1-Br₂** (Figure 4). After 5 min of contact between the electrode and the electrolyte, AFM images

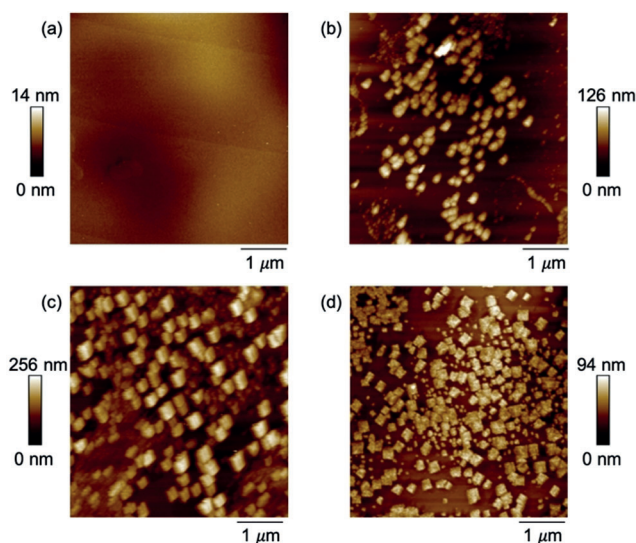


Figure 4. Ex-situ AFM images of Cu electrodes a) after electropolishing; b) after 5 min in contact with a 10 mM solution of **1-Br₂** in 0.1 M KHCO₃; c) after 5 min in contact with a 10 mM solution of **1-Br₂** in 0.1 M KHCO₃ and 3 cycles of PEIS; d) after 65 min of electrocatalysis at -1.07 V in 0.1 M KHCO₃ with **1-Br₂**.

already show some degree of well-defined nanostructuring (Figure 4b), indicating that the bromide anion of the **1-Br₂** additive is effective in corroding the electrode surface. After three cycles of PEIS, AFM images clearly show the presence of well-defined nanostructures (Figure 4c). These observations confirm that the nanostructuring process occurs via corrosion of the copper surface, even before electrocatalysis. As expected, the AFM images taken after electrocatalysis (Figure 4d) show well-defined cubic nanostructures, consistent with the previously discussed SEM images.

To study the effect of the counteranion in the molecular additive, the corresponding phenanthroline ditriflate, dichloride and diiodide molecules were synthesized and tested in CO₂RR ($[1-X_2] = 10$ mM, $X = OTf^-, Cl^-$ and I^- , Table 1 and S6). The **1-(OTf)₂** and **1-Cl₂** derivatives show lower values of total current densities compared with that of **1-Br₂**. Also, the FE for ethylene production decreases 10–15%. Ex-situ post-catalysis AFM images of the electrodes from the experiments with **1-(OTf)₂** and **1-Cl₂** do not show well-defined nanostructures (Figures S18a and S18b). On the other hand, the selectivity of **1-I₂** with respect to ethylene generation is very similar to that with **1-Br₂** ($FE_{C_2H_4} = 43\%$, $j_{C_2H_4} = -1.07$ mA cm⁻²). The overall current density is, however, lower and comparable to that obtained with **1-(OTf)₂** and **1-Cl₂**. Compared to the organic film derived from **1-Br₂**, a thicker film is observable on the electrode when **1-I₂** is used, accounting for the decrease in total current density (Figure S18c). Well-defined nanostructures are observed by AFM after dissolving the film with DMSO (Figure S16d). These observations support previous reports on the incapacity



Table 1: Faradaic efficiency for major products formed during CO₂RR at -1.07 V in CO₂-saturated 0.1 M KHCO₃ without or with 10 mM of **1-X₂** (X = Br, OTf, Cl, I).^[a]

Additive	Faradaic Efficiency [%]				<i>j</i> [mAcm ⁻²]
	H ₂	C ₂ H ₄	C ₂ H ₅ OH	C ₃ H ₇ OH	
None	42.8	12.3	5.9	2.6	-4.5
1-Br₂	15.5	45.4	14.6	3.6	-3.8
1-(OTf)₂	24.1	37.4	14.1	4.9	-2.4
1-Cl₂	25.6	33.8	8.4	5.4	-2.4
1-I₂	21.4	42.0	12.6	4.0	-2.5

[a] All values represent an average of at least two runs. Refer to Table S8 for the complete table.

of Cl⁻ and OTf⁻ anions to effectively corrode copper surfaces, whereas Br⁻ and I⁻ can.^[39,40] Nevertheless, despite the absence of nanostructuring with additives **1-Cl₂** and **1-(OTf)₂**, the improved ethylene selectivity in these systems, compared to bare Cu electrodes, highlights the beneficial effect of the electrodeposition of the organic film onto the surface of the electrode.

To investigate the role of the molecular coating in the stabilization of the observed nanocubes, the organic film from a copper electrode previously subjected to bulk electrolysis in the presence of **1-Br₂** (Figure 5a) was removed by treatment

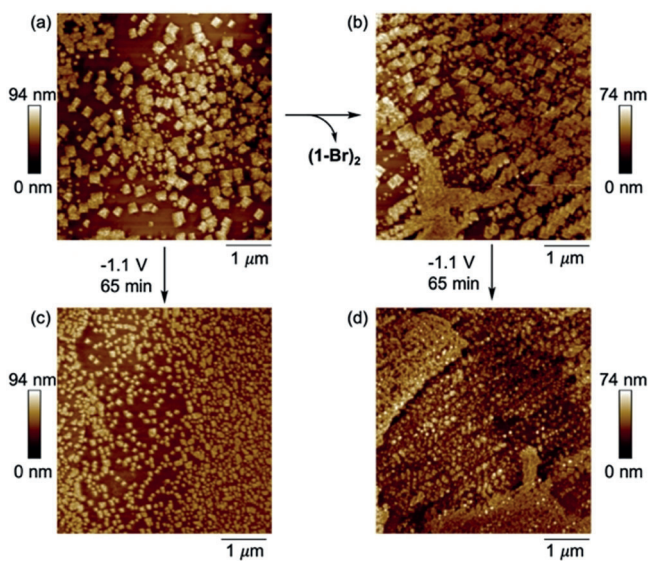


Figure 5. Ex-situ AFM images of Cu electrodes a) after 65 min of electrocatalysis at -1.07 V in 0.1 M KHCO₃ with **1-Br₂**; b) the same electrode as (a) after extracting the organic film; c) after resubmitting a similar electrode as (a) to a second catalytic run; d) after a second catalytic run using same electrode as in (b).

with DMSO. AFM analysis of the resulting electrode shows a decrease in the average height of the nanostructures by ca. 20 nm, potentially due to the removal of the film (Figure 5b). This result suggests that the film thickness is small compared to the size of the copper nanostructures. This nanostructured coating-free electrode was then used in a second bulk electrolysis experiment with an additive-free electrolyte.

The product distribution of this catalytic run shows a considerable reduction in the selectivity for C_{2,2} products, similar to a polycrystalline copper electrode (Table S7). In addition, AFM images of the electrode after the second catalytic run, show degradation of the well-defined nanostructures on the copper surface (Figure 5d). This observation confirms that the electrodeposited organic film plays a critical role in stabilizing the nanostructuring of the electrode under electrocatalytic conditions. This hypothesis is further supported by the finding that the nanostructures are preserved after submitting an electrode functionalized with the organic film to a second catalytic run using an additive-free electrolyte (Figure 5c). As expected, in this experiment not only the nanostructures are preserved, but also the selectivity for C_{2,2} products is similar to the case of the additive-containing electrolyte (Table S8).

The collective observations presented in this work support the conclusion that nanostructuring of the copper electrode, in combination with the electrodeposited organic film, enhances the generation of C_{2,2} products in CO₂RR. This is in agreement with previous studies that have demonstrated the importance of nanostructured Cu surfaces in enhancing selectivity for C_{2,2} products.^[41-43] In contrast to previous reports, using the method reported herein, well-defined cubic nanostructures with exposed {100} facets, known to effectively promote the generation of C-C coupled products,^[44] are not only easily generated, but their morphology is also preserved under electrocatalytic conditions over prolonged reaction times (> 40 h). Besides the stabilizing effect, the molecular coating also plays a role in shifting the selectivity for C-C coupled products, as observed when molecule **1-Cl₂** was used as additive. In this case, since the chloride counteranion failed to corrode the electrode surface to form nanostructures, the increase in the selectivity for ethylene production is due only to the presence of the electrodeposited film.

Figure 6 outlines our working model for the formation and stabilization of the nanostructured copper electrode by a molecular coating derived from **1-Br₂**. Starting from a smooth electrode surface, bromide anions initiate the nanostructuring process by corroding the copper surface and creating nucleation sites. The degree of corrosion is enhanced via PEIS cycles, forming well-defined nanocubes. Upon application of a bias of -1.07 V_{RHE}, reductive dimerization of the phenanthroline dication occurs through coupling of the generated radical (**1-Br**), which is facilitated by the copper surface. This results in the deposition of an organic film onto the electrode. As observed in the SEM and AFM images, this film helps to stabilize the nanostructured surface during electrocatalysis. In addition, the organic film also plays a role in the enhancement of C-C coupling activity.

Conclusion

This study underscores that the combination of an organic halide salt additive, in this case phenanthroline dibromide, with a polycrystalline copper electrode, affords a simple and convenient means to generate and stabilize a nanostructured copper surface for CO₂RR with marked enhancement for

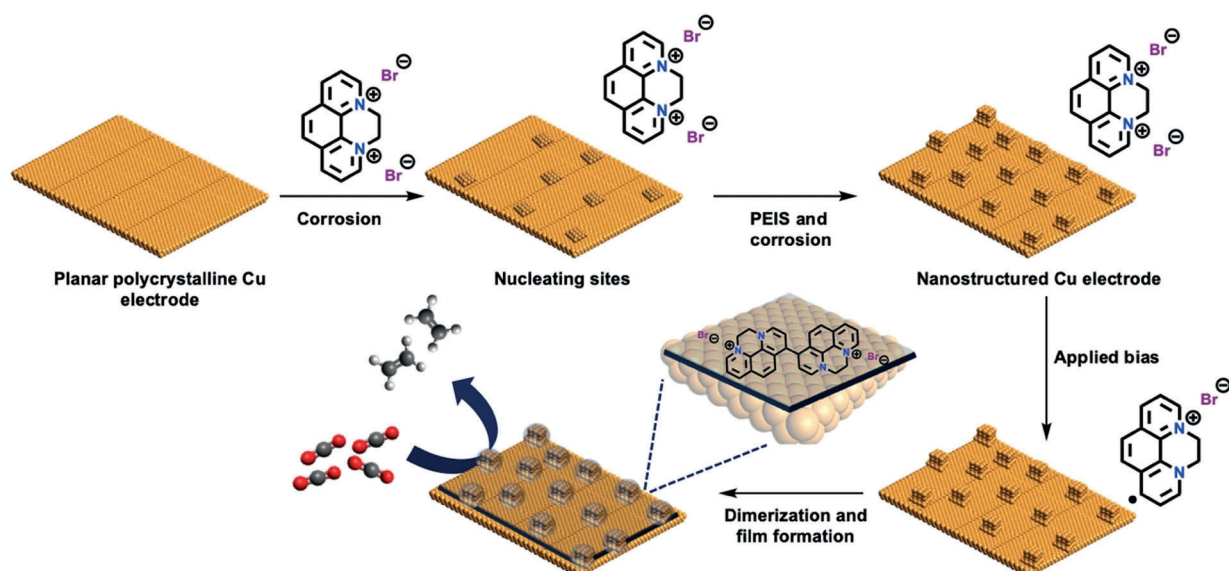


Figure 6. Pictorial representation of the model for nanostructuring of a polycrystalline copper electrode and film electrodeposition as (1-Br)₂. The combination of film and nanostructuring leads to high C₂₋₂ selectivity for CO₂RR electrocatalysis.

C–C coupling, and substantial attenuation of H₂ and especially CH₄. This simple and inexpensive methodology opens promising opportunities for improving CO₂RR through the interaction of organic additives and metal electrodes. Preserving nanostructures during catalysis, as demonstrated here, is important beyond CO₂RR and may find applications to a variety of electrocatalysts already reported in the literature.

Acknowledgements

NMR, AFM and XPS, SEM and EDX measurements were collected at the NMR Facility (Division of CCE), the Molecular Materials Research Center (Beckman Institute) and the Analytic Facilities (Division of Geological and Planetary Sciences) of the California Institute of Technology, respectively. This material is based upon work performed by the Joint Center for Artificial Photosynthesis, a DOE Energy Innovation Hub, supported through the Office of Science of the U.S. Department of Energy under Award Number DE-SC0004993 and Marie Curie Fellowship H2020-MSCA-IF-2017 (793471) (A.T.). J.C.P. acknowledges additional support from the Resnick Sustainability Institute at Caltech.

Conflict of interest

The authors declare no conflict of interest.

Keywords: carbon dioxide · electrocatalysis · ethylene · nanocubes · stability

- [1] X. Cui, W. Li, P. Ryabchuk, K. Junge, M. Beller, *Nat. Catal.* **2018**, *1*, 385–397.
- [2] C. Copéret, F. Allouche, K. W. Chan, M. P. Conley, M. F. Delley, A. Fedorov, I. B. Moroz, V. Mougel, M. Pucino, K. Searles, et al., *Angew. Chem. Int. Ed.* **2018**, *57*, 6398–6440; *Angew. Chem.* **2018**, *130*, 6506–6551.
- [3] J. D. A. Pelletier, J.-M. Basset, *Acc. Chem. Res.* **2016**, *49*, 664–677.
- [4] C. Copéret, M. Chabanas, R. Petroff Saint-Arroman, J.-M. Basset, *Angew. Chem. Int. Ed.* **2003**, *42*, 156–181; *Angew. Chem.* **2003**, *115*, 164–191.
- [5] Z. Han, R. Kortlever, H.-Y. Chen, J. C. Peters, T. Agapie, *ACS Cent. Sci.* **2017**, *3*, 853–859.
- [6] B. A. Rosen, A. Salehi-Khojin, M. R. Thorson, W. Zhu, D. T. Whipple, P. J. A. Kenis, R. I. Masel, *Science* **2011**, *334*, 643–644.
- [7] Z. Cao, J. S. Derrick, J. Xu, R. Gao, M. Gong, E. M. Nichols, P. T. Smith, X. Liu, X. Wen, C. Copéret, et al., *Angew. Chem. Int. Ed.* **2018**, *57*, 4981–4985; *Angew. Chem.* **2018**, *130*, 5075–5079.
- [8] G. P. S. Lau, M. Schreier, D. Vasilyev, R. Scopelliti, M. Grätzel, P. J. Dyson, *J. Am. Chem. Soc.* **2016**, *138*, 7820–7823.
- [9] C. Kim, H. S. Jeon, T. Eom, M. S. Jee, H. Kim, C. M. Friend, B. K. Min, Y. J. Hwang, *J. Am. Chem. Soc.* **2015**, *137*, 13844–13850.
- [10] C. Kim, T. Eom, M. S. Jee, H. Jung, H. Kim, B. K. Min, Y. J. Hwang, *ACS Catal.* **2017**, *7*, 779–785.
- [11] M. Gong, Z. Cao, W. Liu, E. M. Nichols, P. T. Smith, J. S. Derrick, Y.-S. Liu, J. Liu, X. Wen, C. J. Chang, *ACS Cent. Sci.* **2017**, *3*, 1032–1040.
- [12] S. Ponnurangam, I. V. Chernyshova, P. Somasundaran, *Adv. Colloid Interface Sci.* **2017**, *244*, 184–198.
- [13] L. Zhang, Z.-J. Zhao, J. Gong, *Angew. Chem. Int. Ed.* **2017**, *56*, 11326–11353; *Angew. Chem.* **2017**, *129*, 11482–11511.
- [14] M. Ma, W. A. Smith in *Anisotropic and Shape-Selective Nanomaterials: Structure-Property Relationships* (Eds.: S. E. Hunyadi Murph, G. K. Larsen, K. J. Coopersmith), Springer International Publishing, Cham, **2017**, pp. 337–373.
- [15] H. Mistry, A. S. Varela, S. Köhl, P. Strasser, B. R. Cuenya, *Nat. Rev. Mater.* **2016**, *1*, 16009.

- [16] P. Grosse, D. Gao, F. Scholten, I. Sinev, H. Mistry, B. Roldan Cuenya, *Angew. Chem. Int. Ed.* **2018**, *57*, 6192–6197; *Angew. Chem.* **2018**, *130*, 6300–6305.
- [17] D. Gao, F. Scholten, B. Roldan Cuenya, *ACS Catal.* **2017**, *7*, 5112–5120.
- [18] C. Reller, R. Krause, E. Volkova, B. Schmid, S. Neubauer, A. Rucki, M. Schuster, G. Schmid, *Adv. Energy Mater.* **2017**, *7*, 1602114.
- [19] R. M. Arán-Ais, D. Gao, B. Roldan Cuenya, *Acc. Chem. Res.* **2018**, *51*, 2906–2917.
- [20] C. W. Li, M. W. Kanan, *J. Am. Chem. Soc.* **2012**, *134*, 7231–7234.
- [21] H. Mistry, A. S. Varela, C. S. Bonifacio, I. Zegkinoglou, I. Sinev, Y.-W. Choi, K. Kisslinger, E. A. Stach, J. C. Yang, P. Strasser, et al., *Nat. Commun.* **2016**, *7*, 12123.
- [22] D. Gao, I. Zegkinoglou, N. J. Divins, F. Scholten, I. Sinev, P. Grosse, B. Roldan Cuenya, *ACS Nano* **2017**, *11*, 4825–4831.
- [23] H. S. Jeon, S. Kunze, F. Scholten, B. Roldan Cuenya, *ACS Catal.* **2018**, *8*, 531–535.
- [24] D. Kim, C. S. Kley, Y. Li, P. Yang, *Proc. Natl. Acad. Sci. USA* **2017**, *114*, 10560–10565.
- [25] A. S. Hall, Y. Yoon, A. Wuttig, Y. Surendranath, *J. Am. Chem. Soc.* **2015**, *137*, 14834–14837.
- [26] Y. Li, F. Cui, M. B. Ross, D. Kim, Y. Sun, P. Yang, *Nano Lett.* **2017**, *17*, 1312–1317.
- [27] P. Lobaccaro, M. R. Singh, E. L. Clark, Y. Kwon, A. T. Bell, J. W. Ager, *Phys. Chem. Chem. Phys.* **2016**, *18*, 26777–26785.
- [28] K. P. Kuhl, E. R. Cave, D. N. Abram, T. F. Jaramillo, *Energy Environ. Sci.* **2012**, *5*, 7050–7059.
- [29] Y. Hori in *Modern Aspects of Electrochemistry* (Eds.: C. G. Vayenas, R. E. White, M. E. Gamboa-Aldeco), Springer, New York, **2008**, pp. 89–189.
- [30] A. Wuttig, Y. Surendranath, *ACS Catal.* **2015**, *5*, 4479–4484.
- [31] S. Men, D. S. Mitchell, K. R. J. Lovelock, P. Licence, *ChemPhys-Chem* **2015**, *16*, 2211–2218.
- [32] Y. Zhao, X. Liu, Y. Han, *RSC Adv.* **2015**, *5*, 30310–30330.
- [33] A. P. Shaw, B. L. Ryland, M. J. Franklin, J. R. Norton, J. Y.-C. Chen, M. L. Hall, *J. Org. Chem.* **2008**, *73*, 9668–9674.
- [34] The balance of the organic material could correspond to unidentified by-products and other diastereoisomers of the *ortho-ortho* and *para-para* dimers (**1-Br**).
- [35] A. N. Karaiskakis, E. J. Biddinger, *Energy Technol.* **2017**, *5*, 901–910.
- [36] S. Ogata, N. Kobayashi, T. Kitagawa, S. Shima, A. Fukunaga, C. Takatoh, T. Fukuma, *Corros. Sci.* **2016**, *105*, 177–182.
- [37] Y. Kwon, Y. Lum, E. L. Clark, J. W. Ager, A. T. Bell, *Chem-ElectroChem* **2016**, *3*, 1012–1019.
- [38] F. S. Roberts, K. P. Kuhl, A. Nilsson, *Angew. Chem. Int. Ed.* **2015**, *54*, 5179–5182; *Angew. Chem.* **2015**, *127*, 5268–5271.
- [39] I. T. McCrum, S. A. Akhade, M. J. Janik, *Electrochim. Acta* **2015**, *173*, 302–309.
- [40] A. S. Varela, W. Ju, T. Reier, P. Strasser, *ACS Catal.* **2016**, *6*, 2136–2144.
- [41] T. Saberi Safaei, A. Mephram, X. Zheng, Y. Pang, C.-T. Dinh, M. Liu, D. Sinton, S. O. Kelley, E. H. Sargent, *Nano Lett.* **2016**, *16*, 7224–7228.
- [42] M. Ma, K. Djanashvili, W. A. Smith, *Angew. Chem. Int. Ed.* **2016**, *55*, 6680–6684; *Angew. Chem.* **2016**, *128*, 6792–6796.
- [43] P. De Luna, R. Quintero-Bermudez, C.-T. Dinh, M. B. Ross, O. S. Bushuyev, P. Todorović, T. Regier, S. O. Kelley, P. Yang, E. H. Sargent, *Nat. Catal.* **2018**, *1*, 103–110.
- [44] C. Hahn, T. Hatsukade, Y.-G. Kim, A. Vailionis, J. H. Baricuatro, D. C. Higgins, S. A. Nitopi, M. P. Soriaga, T. F. Jaramillo, *Proc. Natl. Acad. Sci. USA* **2017**, *114*, 5918–5923.

Manuscript received: June 25, 2019

Revised manuscript received: August 13, 2019

Accepted manuscript online: September 19, 2019

Version of record online: ■ ■ ■ ■ ■ ■ ■ ■ ■ ■



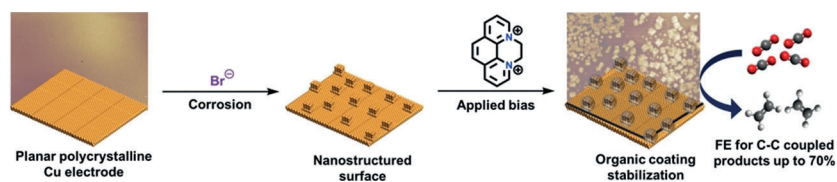
Research Articles



Electrocatalysis

A. Thevenon, A. Rosas-Hernández,
J. C. Peters,* T. Agapie* — ■■■■—■■■■

In-Situ Nanostructuring and Stabilization
of Polycrystalline Copper by an Organic
Salt Additive Promotes Electrocatalytic
CO₂ Reduction to Ethylene



Catalytic cubes: An efficient method for nanostructuring copper electrodes using *N,N'*-ethylene-phenanthroline dibromide as a molecular additive is reported. Using such Cu electrodes in electro-

chemical CO₂ reduction produces C_{≥2} products with selectivities up to 70% for more than 40 h without significant change in the surface morphology.